Desalination and Water Treatment
www.deswater.com

doi: 10.5004/dwt.2017.21678

97 (2017) 191–202
November

Fabrication and characterization of pyrophyllite-based ceramic membranes: filtration experiments with pure water, bovine serum albumin solution, and oil-in-water emulsion

Eun-Hye Sim[a], Jin-Kyu Kang[a], Seung-Chan Lee[a], Nag-Choul Choi[a], Song-Bae Kim[a,b,*], Cheon-Young Park[c]

[a]*Environmental Functional Materials and Water Treatment Laboratory, Seoul National University, Korea, Tel. +82-2-880-4587; email: songbkim@snu.ac.kr (S.-B. Kim)*
[b]*Department of Rural Systems Engineering and Research Institute of Agriculture and Life Sciences, Seoul National University, Korea*
[c]*Department of Energy and Resource Engineering, Chosun University, Korea*

Received 29 June 2017; Accepted 13 November 2017

ABSTRACT

Pyrophyllite-based ceramic membranes with an alumina coating layer were fabricated in this study. Filtration experiments with pure water, bovine serum albumin (BSA) solution, and oil-in-water (OW) emulsion were performed to characterize the filtration properties of the membranes. In the filtration experiments with pure water, the hydraulic permeability and pore radius of the membranes were determined to be 1.55×10^{-6} m^3/m^2 s kPa and 1.1×10^{-7} m, respectively. In the filtration experiments with BSA solution, the rejection rates of BSA solution in the membranes were very low (7.2%–16.1%). These results were attributed to the far smaller particle size of the BSA (11 nm) than the pore size of the membranes. In the filtration experiments with OW emulsion, the rejection rates of OW emulsion were very high (72.3%–91.8%) because the size of the oil droplets (250–490 nm) was larger than the pore size of the membranes. Five combined fouling models of cake-complete, cake-intermediate, complete-standard, intermediate-standard, and cake-standard were used to analyze the BSA and OW emulsion filtration data.

Keywords: Bovine serum albumin solution; Ceramic membrane filtration; Combined fouling model analysis; Oil-in-water emulsion; Pyrophyllite-based ceramic membrane

1. Introduction

Polymeric and ceramic membrane filtrations have been applied as advanced technologies for water and wastewater treatment [1]. Recently, ceramic membranes have gained considerable attention due to their superior properties relative to polymeric membranes, including chemical resistance, thermal stability, mechanical strength, and hydrophilicity [2]. Ceramic membranes are composed of a support layer and a thin active layer, which are made of inorganic materials, such as alumina (Al_2O_3), zirconia (ZrO_2), titania (TiO_2), silica (SiO_2), and silicon carbide (SiC). Among these, alumina is primarily used for the preparation of ceramic membrane supports [3]. However, alumina-based ceramic membranes are not suitable for large application because of the high cost of both starting materials and sintering process [4]. Therefore, low-cost clay materials have been used by many researchers to fabricate the membrane supports [5–13].

Pyrophyllite ($Al_2Si_4O_{10}(OH)_2$) is a 2:1 hydrous aluminosilicate clay with a dioctahedral layer structure with octahedrally coordinated Al ion sheets between two sheets of SiO_4 tetrahedra [14]. Pyrophyllite has been used as a raw material in the ceramic, glass, and refractory industries [15]. Recently, researchers have used pyrophyllite as a low-cost material

* Corresponding author.

for the fabrication of ceramic membrane supports [16]. A research group from India [17] prepared clay-based membrane supports from clay mixtures that included a minor portion (10–15 wt%) of pyrophyllite. They used the fabricated ceramic membranes for the separation of hexavalent chromium [18], electrolytes [19,20], bovine serum albumin (BSA) [21], and oily wastewater [21–23]. Monash and Pugazhenthi [21] have fabricated three ceramic membrane supports (I, 3G, and 6G) with different compositions of raw materials (kaolin, ball clay, feldspar, pyrophyllite, calcium carbonate, quartz, and titanium dioxide). They used the membrane supports for the separation experiments of oil-in-water (OW) emulsion and BSA solution, reporting that a maximum rejection rate of 99% was obtained with 6G support for OW emulsion, whereas a maximum rejection rate of 40% was obtained with 6G support for BSA solution. Kumar et al. [23] have fabricated ceramic membrane supports using inexpensive clay mixtures of kaolin, ball clay, feldspar, pyrophyllite, quartz, and calcium carbonate and applied the supports to microfiltration of synthetic oily wastewater. They reported that the highest rejection rate of 99.98% was obtained at the applied pressure of 69 kPa.

Another group from the Republic of Korea fabricated pyrophyllite-based membrane supports using pyrophyllite as a support material and diatomite as a pore forming agent [24–26]. Ha et al. [24] have fabricated pyrophyllite–diatomite composite supports with different amount of diatomite to examine the effect of diatomite as a pore forming agent on the pore size and permeability of the composite supports. They reported that the pore characteristics of the composite supports could be easily controlled through the addition of diatomite. Ha et al. [26] have prepared alumina-coated alumina supports and alumina-coated pyrophyllite–diatomite composite supports to compare the pore size and permeability of those membranes using mercury porosimetry and water permeability test. Even though the pyrophyllite-based membranes were fabricated by the Korean research group, their studies were limited to the characterization of the physical properties of the pyrophyllite membrane supports, such as pore size, flexural strength, and permeability.

Therefore, pyrophyllite-based ceramic membranes with an alumina coating layer were fabricated in this study using pyrophyllite as a major support material. Filtration experiments with pure water, BSA solution, and OW emulsion were performed to characterize the filtration properties of the pyrophyllite-based membranes. In addition, the characteristics of the pyrophyllite-based ceramic membranes were analyzed by various techniques, including field emission scanning electron microscopy (FESEM), energy-dispersive X-ray spectrometry (EDS), and X-ray diffractometry (XRD).

2. Materials and methods

2.1. Fabrication and characterization of pyrophyllite-based ceramic membranes

Pyrophyllite was obtained from the Sungsan Mine (Haenam, Republic of Korea). The physicochemical characteristics of pyrophyllite were presented in our previous study [27]. Flat tubular-type membrane supports (non-layered membranes) were made by extruding a mixture of 80% pyrophyllite (particle size =2–40 μm), 20% α-alumina (particle size = 2–3 μm), 2% graphite (particle size = 10 μm), and water using an extruder (IB Materials, Yeongam, Republic of Korea). Note that the pore size of ceramic membranes can be controlled by the particle size of pore-forming agent [28]. In this study, a micron-sized graphite was used as a pore forming agent to prepare the membrane supports with pore diameter suitable for microfiltration. The extruded membrane supports were dried using a two-step method (microwave and hot air) and were then sintered at 1,350°C for 2 h.

Alumina-coated pyrophyllite membranes (layered membranes) were prepared from the membrane supports by coating a thin layer over the supports using a dip-coating method. The membrane supports were dipped into the dip-coating solutions containing alumina (8 wt%), isopropyl alcohol (33 wt%), AP-2 binder (2 wt%), and water (57 wt%). The alumina-coated membranes were dried at 80°C for 12 h and then sintered at 1,350°C for 2 h [29].

The morphology and elemental composition of the ceramic membranes were examined by FESEM and EDX analyses (Supra 55VP, Carl Zeiss, Oberkochen, Germany), respectively. The mineralogical and crystalline structural properties of the membranes were determined by XRD analysis (D8 Advance, Bruker, Karlsruhe, Germany) with Cu Kα radiation (λ = 1.5418 Å) at a scanning speed of 0.5 s/step. The flexural strengths of the membranes were measured by a three-point bending test (DTU-900 MHA, Daekyung Tech & Testers, Incheon, Republic of Korea).

2.2. Ceramic membrane system

A schematic illustration of the submerged ceramic filtration system used in the test is presented in Fig. 1. The ceramic filtration unit consisted of a feed tank, a membrane tank, a permeate tank, a pressure transmitter, peristaltic pumps, and flow meters. The membrane tank is a cubic acrylic tank with dimensions of 220 cm (length) × 110 cm (width) × 458 cm (height). The ceramic membrane was submerged and vertically fixed in the membrane tank. Two (feed and suction) peristaltic pumps (CT3001F, Lead Fluid, Baoding City, China) were operated at the same rate to maintain a constant water level in the membrane tank. The pressure transmitter (SXT series, ULFA Technology Co., Seoul, Republic of Korea) was installed between the membrane and the peristaltic pump to monitor the transmembrane pressure (TMP). Two flow meters (MX06-MX100, Macnaught, Turrella, NSW, Australia)

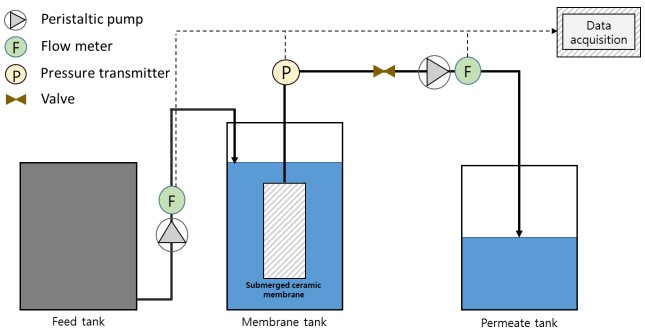

Fig. 1. A schematic diagram of the submerged ceramic membrane system.

were installed on the peristaltic pumps to monitor the water flux. The pressure and permeate flux data from the pressure transmitter and flow meters were automatically recorded on a computer.

2.3. Filtration experiments with pure water

Prior to water permeation experiments, the porosity (n, %) of the membranes was determined by the Archimedes' method along with the following relationship [30]:

$$n = \frac{M_w - M_d}{M_w - M_a} \quad (1)$$

In addition, water permeation experiments were conducted at room temperature with deionized water under a constant flow rate (Q = 8.33 × 10^{-7} to 3.33 × 10^{-6} m^3/s) in order to determine the hydraulic permeability (H_p, m^3/m^2 s kPa) and hydraulic pore radius (H_r, m) of the pyrophyllite-based ceramic membranes, which are calculated as follows [30]:

$$H_p = \frac{Q}{A\Delta P} \quad (2)$$

$$H_r = \sqrt{\frac{8\mu d H_p}{n}} \quad (3)$$

where A is the effective membrane area (m^2), ΔP is the TMP (kPa), μ is the viscosity of water (kPa s), and d is the membrane thickness (m).

2.4. Filtration experiments with BSA solution

BSA solution filtration experiments were performed under a constant flow rate at room temperature. BSA was chosen to represent a typical protein-like substance, which is one of the major membrane foulants [31]. BSA (pH 7, ≥98%) was purchased from Sigma-Aldrich (Saint Louis, MO, USA). The BSA solutions were prepared by dissolving a given amount (200, 500, and 1,000 mg/L) of BSA powder in deionized water and then stirring for 6 h. The experimental conditions are summarized in Table 1. Experiments 1–3 were performed at a flow rate ranging from 8.33 × 10^{-7} to 2.50 × 10^{-6} m^3/s with a BSA concentration of 200 mg/L. These experiments were continued until 3.5 L of permeate were collected. Additional experiments (Exps. 4 and 5) were conducted at a flow rate of 1.67 × 10^{-6} m^3/s with a BSA concentration of 500 or 1,000 mg/L and a filtration time of 90 min. The BSA concentration in the feed water and permeate was measured using a UV–visible spectrometer (Genesys 10S, Thermo Scientific, Waltham, MA, USA) at a wavelength of 595 nm according to the Bradford protein assay with Bradford reagent (Sigma-Aldrich). The rejection rate (R, %) was calculated using the following relationship:

$$R = \frac{C_i - C_p}{C_i} \times 100 \quad (4)$$

After the each filtration experiment, the fouled membrane was chemically cleaned using alkaline cleaning and acid cleaning to recover the initial permeability. The membrane was immersed in NaOH solution (10 g/L) for 120 min at 39°C. Then, the membrane was washed thoroughly with deionized water. Thereafter, the membrane was immersed in HNO_3 solution (5 mL/L) for 30 min at 39°C. Then, the membrane was washed thoroughly with deionized water. After completion of membrane cleaning, the water permeability of the cleaned membrane was tested with deionized water at the constant flow rate to confirm the recovery of water permeability (97% of recovery).

2.5. Filtration experiments with OW emulsion

OW emulsion filtration experiments were conducted under a constant flow rate at room temperature. Soybean oil (density = 0.92 g/mL) and sodium dodecyl sulfate (surfactant, ≥90%) purchased from Sigma-Aldrich were used in the experiments. The OW emulsions were prepared by mixing a given amount of soybean oil (50, 100, and 200 mg/L) and sodium dodecyl sulfate (10 mg/L) with deionized water. Stable OW emulsions were generated by sonication for 6 h using a ultrasonicator (Q500, Qsonica, Newton, CT, USA). The size distribution of oil droplets in the emulsions was measured using a particle size analyzer (Mastersizer 2000, Malvern Instruments, Malvern, UK). The experimental conditions are

Table 1
Experimental conditions and results of bovine serum albumin (BSA) solution and oil-in-water (OW) emulsion filtration

Exp.	Solution	Solution concentration (mg/L)	Flow rate (m^3/s)	Volume of feed (mL)	Filtration time (min)	Rejection rate (%)
1	BSA	200	8.33 × 10^{-7}	3,500	100	11.0
2	BSA	200	1.67 × 10^{-6}	3,500	47	10.6
3	BSA	200	2.50 × 10^{-6}	3,500	31	11.3
4	BSA	500	1.67 × 10^{-6}	6,000	100	16.1
5	BSA	1,000	1.67 × 10^{-6}	6,000	100	7.2
6	OW	200	8.33 × 10^{-7}	400	90	90.4
7	OW	200	1.67 × 10^{-6}	400	71	86.7
8	OW	200	2.50 × 10^{-6}	400	17	91.8
9	OW	50	1.67 × 10^{-6}	3,000	90	72.3
10	OW	100	1.67 × 10^{-6}	1,100	90	81.7

also summarized in Table 1. For Exps. 6–8, filtration was conducted at a flow rate ranging from 8.33×10^{-7} to 2.50×10^{-6} m^3/s with an OW emulsion concentration of 200 mg/L. The experiments were continued until 0.4 L of permeate were collected. Additional experiments (Exps. 9 and 10) were performed at a flow rate of 1.67×10^{-6} m^3/s with OW emulsion concentrations of 50 and 100 mg/L and a filtration time of 90 min. The oil concentration in the feed water and permeate was analyzed using a total organic carbon analyzer (Sievers 5310C, GE Analytical Instruments, Boulder, CO, USA). After the each filtration experiment, the fouled membrane was chemically cleaned using 1% detergent solution for 30 min. Then, the cleaned membrane was washed thoroughly with deionized water for 30 min. After completion of membrane cleaning, the water permeability of the cleaned membrane was tested by following the same procedure described in the BSA filtration test (97% of recovery).

2.6. Combined fouling models

Hermia [32] derived the blocking filtration laws to describe fouling mechanisms during constant pressure membrane filtration. Four individual pore blocking models were presented in that work, including the complete blocking filtration model, the intermediate blocking filtration model, the standard blocking filtration model, and the cake filtration model. However, the individual fouling model is not accurate enough to describe the membrane fouling mechanism because membrane fouling can be caused by a combination of several individual fouling mechanism [33].

Bolton et al. [34] combined the individual fouling models into a combined fouling model that includes cake-complete, cake-intermediate, complete-standard, intermediate-standard, and cake-standard models. Several researchers [35–38] have used the combined models to analyze the membrane fouling mechanism during membrane filtration. The five combined fouling models for constant flow operation can be presented as follows [34]:

$$\frac{P_t}{P_0} = \frac{1}{1-K_b t}\left(1 - \frac{K_c J_0^2}{K_b}\ln(1-K_b t)\right) \quad \text{Cake-complete model} \tag{5}$$

$$\frac{P_t}{P_0} = \exp(K_i J_0 t)\left(1 + \frac{K_c J_0}{K_i}(\exp(K_i J_0 t) - 1)\right) \tag{6}$$

Cake-intermediate model

$$\frac{P_t}{P_0} = \frac{1}{(1-K_b t)(1+(K_s J_0/2K_b)\ln(1-K_b t))^2} \tag{7}$$

Complete-standard model

$$\frac{P_t}{P_0} = \frac{\exp(K_i J_0 t)}{(1-(K_s/2K_i)(\exp(K_i J_0 t)-1))^2} \tag{8}$$

Intermediate-standard model

$$\frac{P_t}{P_0} = \left(1 - \frac{K_s J_0 t}{2}\right)^{-2} + K_c J_0^2 t \quad \text{Cake-standard model} \tag{9}$$

The error functions, including the sum of the absolute error (SAE), Marquardt's percentage standard deviation (MPSD), and determination coefficient (R^2), are used in the model analysis:

$$\text{SAE} = \sum_{i=1}^{n} \left| y_c - y_e \right|_i \tag{10}$$

$$\text{MPSD} = 100\sqrt{\frac{1}{n-1}\sum_{i=1}^{n}\left(\frac{y_c - y_e}{y_e}\right)_i^2} \tag{11}$$

$$R^2 = \frac{\sum_{i=1}^{m}\left(y_c - \overline{y_e}\right)_i^2}{\sum_{i=1}^{m}\left(y_c - \overline{y_e}\right)_i^2 + \sum_{i=1}^{m}\left(y_c - y_e\right)_i^2} \tag{12}$$

In this study, model Eqs. (5)–(9) were used to analyze the filtration data for the BSA solution and OW emulsion by non-linear regression using error functions of Eqs. (10)–(12).

3. Results and discussion

3.1. FESEM, EDX, and XRD

The characteristics of the pyrophyllite-based ceramic membranes are shown in Fig. 2. Physical characteristics of the ceramic membrane supports are summarized in Table 2. The ceramic membrane supports had dimensions of 240 mm (length) × 75 mm (width) with an effective membrane area of 0.0379 m^2. The FESEM images demonstrated the heterogeneous surface morphology of the non-layered (Fig. 2(a)) and layered (Fig. 2(d)) membranes. The flat tubular-type modules of the non-layered and layered membranes are shown in the insets of Figs. 2(a) and (d), respectively. The cross-sectional FESEM images (Figs. 2(b) and (e)) show that the ceramic membranes were composed of a membrane support (thickness = 4 mm) and an alumina coating layer (thickness = 7.16 μm).

The EDX patterns (Figs. 2(c) and (f)) indicated that silica (Si) and carbon (C) were the major elements of the ceramic membranes. The atomic percentage of aluminum (Al) in the layered membranes was 11.48%, which was far higher than that (0.83%) in the non-layered membranes due to the alumina coating layer.

The XRD patterns of the non-layered and layered membranes are presented in Fig. 3. Pyrophyllite was mainly composed of silica and alumina. During fabrication of the ceramic membranes, the general XRD pattern of pyrophyllite disappeared because pyrophyllite was sintered at 1,350°C. Quartz (SiO_2, hexagonal) and cristobalite (SiO_2, tetragonal) were observed to be the major phases in the non-layered and layered membranes, respectively. In addition, peaks of mullite ($Al_6Si_2O_{13}$) and corundum (Al_2O_3) were observed. Similar findings were reported by Ha et al. [24], who observed the appearance of peaks for quartz, cristobalite, and mullite when the pyrophyllite support layer was sintered at 1,300°C.

3.2. Water permeation experiments

The TMP vs. pure water flow rate in pyrophyllite-based membranes is presented in Fig. 4 to determine the relationship

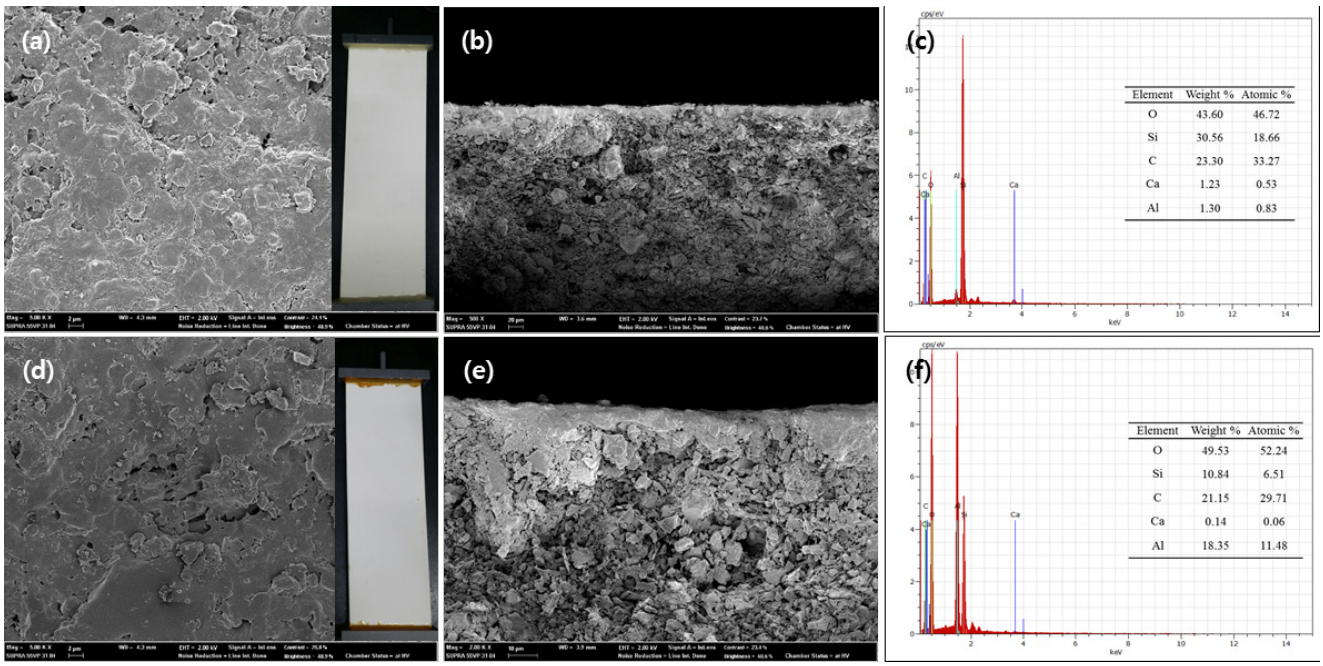

Fig. 2. Characteristics of pyrophyllite-based membranes: (a) FESEM of non-layered membrane surface (bar = 2 μm; inset = digital image of non-layered membrane module), (b) FESEM of non-layered membrane (cross-section, bar = 2 μm), (c) EDS pattern of non-layered membrane (inset = elemental composition), (d) FESEM of layered membrane surface (bar = 2 μm; inset = digital image of layered (alumina-coated) membrane module), (e) FESEM of layered membrane (cross-section, bar = 2 μm), and (f) EDS pattern of layered membrane (inset = elemental composition).

Table 2
Physical characteristics of pyrophyllite-based membrane support fabricated in this study

Type	Flat tubular
Filtration direction	Out–in
Length (mm)	240
Width (mm)	75
Thickness of support (mm)	4
Effective membrane area (m^2)	0.379
Flexural strength (MPa)	29.1

between hydraulic permeability and hydraulic pore radius. The hydraulic permeabilities of the non-layered and layered membranes were 2.21×10^{-6} and 1.55×10^{-6} m^3/m^2 s kPa, respectively, indicating that the permeability of the membranes was reduced due to the presence of the coating layer. The average pore radii of the non-layered and layered membranes were 1.2×10^{-7} and 1.1×10^{-7} m, respectively. From the Archimedes' method, the porosity of the non-layered membranes was determined to be 47.0%, whereas the porosity of the layered membranes was 36.3% due to the alumina coating layer.

The values of hydraulic permeability and pore radius from this study were comparable with the values reported in the literature (Table 3) [26,30,39–43]. Ha et al. [26] reported that the hydraulic permeabilities of the non-layered and layered pyrophyllite–diatomite membranes were 8.34×10^{-6} and 2.78×10^{-6} m^3/m^2 s kPa, respectively, whereas the average pore radii of the membranes were 5.1×10^{-7} and 5.5×10^{-8} m, respectively.

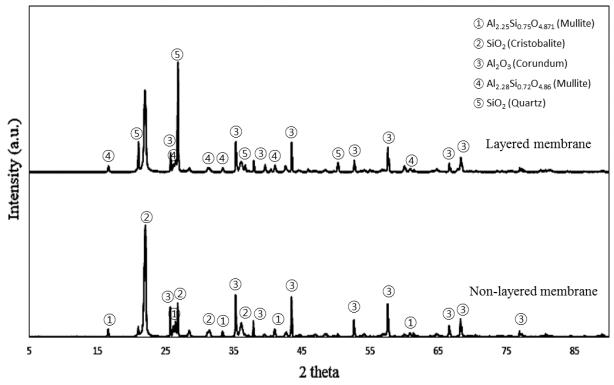

Fig. 3. XRD patterns of pyrophyllite-based membranes.

3.3. BSA solution filtration

The permeate volume vs. TMP for BSA solution filtration are shown in Fig. 5. The rejection rates for the BSA solution are presented in Table 1. BSA filtration experiments (Exps. 1, 2, and 3) were performed at three different flow rates with a permeate volume of 3.5 L. In Exp. 1 (BSA concentration = 200 mg/L, flow rate = 8.33×10^{-7} m^3/s), the TMP values remained relatively constant at 12–13 kPa throughout the BSA solution filtration. The rejection rate of BSA solution was determined to be 11.0%. As the flow rate increased, the TMP values remained relatively constant at higher values throughout the filtration. For Exp. 2 (BSA concentration = 200 mg/L, flow rate = 1.67×10^{-6} m^3/s), the TMP values remained at 21–22 kPa with a rejection rate of 10.6%. In Exp. 3 (BSA concentration = 200 mg/L, flow rate = 2.50×10^{-6} m^3/s),

the TMP values remained at 35–37 kPa with a rejection rate of 10.6%. Our results indicate that the rejection rate of BSA solution was not affected by the applied flow rate under the given experimental conditions.

Additional experiments (Exps. 4 and 5) were conducted with two different concentrations of BSA solution and a filtration time of 90 min. In Exp. 4 (BSA concentration = 500 mg/L, flow rate = 1.67×10^{-6} m^3/s), the TMP values remained at 23–24 kPa with a rejection rate of 16.1%. For Exp. 5 (BSA concentration = 1,000 mg/L, flow rate = 1.67×10^{-6} m^3/s), the TMP values remained at 24–25 kPa with a rejection rate of 7.2%, which was lower than that of Exp. 4.

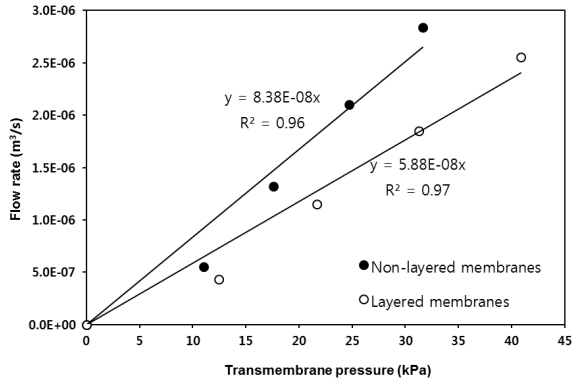

Fig. 4. Transmembrane pressure (TMP) vs. pure water flow rate in pyrophyllite-based membranes.

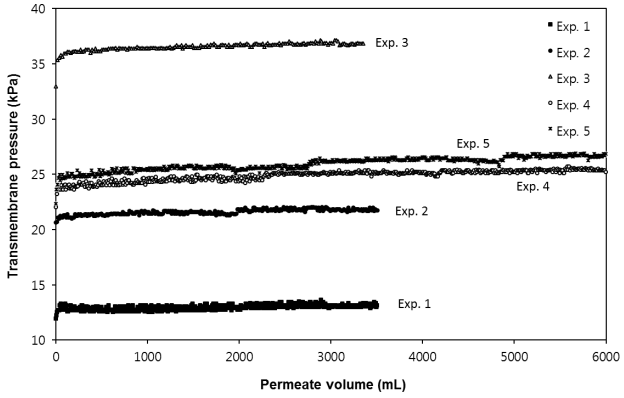

Fig. 5. Bovine serum albumin (BSA) solution filtration (permeate volume vs. transmembrane pressure (TMP) data).

Our results demonstrated that the rejection rates of BSA solution were very low (7.2%–16.1%) and remained relatively constant under a given set of experimental conditions. These results were attributed to the far smaller particle size of the BSA than the pore diameter of the pyrophyllite-based ceramic membranes. It is known that BSA contains prolate ellipsoids with dimensions of 140 × 40 × 40 $Å^3$ [44]. BSA has a molecular weight of 66,430 Da [45], which was calculated to be 11.0nm from the equation in the literature [46]. Note that the average pore diameter of the layered ceramic membranes used in this study was 220 nm (Table 3), which was 22 times larger than the size of the BSA. Therefore, BSA particles could easily pass through the ceramic membranes during the filtration experiments. Similar findings have been reported by Monash and Pugazhenthi [21] demonstrated that, under the given experimental conditions (BSA concentration = 500 mg/L, solution pH = 7.0), the BSA rejection rates were very low (I support = 1%–9%, 3G support = 3%–10%, and 6G support = 5%–16%), showing a decreasing tendency with an increase in applied pressure from 69 to 345 kPa. At an applied pressure of 207 kPa, the rejection rates decreased (I support = 6%–16%, 3G support = 11%–27%, and 6G support = 18%–40%) with an increase in the BSA concentration from 100 to 400 mg/L. At BSA concentrations ranging from 500 to 3,000 mg/L, however, the rejection rates remained relatively constant (I support = 3%–6%, 3G support = 6%–8%, and 6G support = 10%–16%). Vasanth et al. [47] fabricated ceramic–LTA zeolite composite membranes (Z1–Z4) and applied Z4 membranes (average pore size = 76 nm) for ultrafiltration of BSA solutions. They reported that the BSA rejection rate was highest at pH 2.5 (80%) at an applied pressure of 207 kPa and decreased sharply with an increase in pH to 5.0, finally reaching 1% at a solution pH of 6.3–8.0. The BSA rejection rate decreased from 80% to 54% with an increase in applied pressure from 207 to 345 kPa.

Table 3
Comparison of pore radius and hydraulic permeability reported in the literature

Major support material	Pore radius (m)	Hydraulic permeability (m^3/m^2 s kPa)	Reference
Pyrophyllite (non-layered)	1.2×10^{-7}	2.21×10^{-6}	This work
Pyrophyllite (layered)	1.1×10^{-7}	1.55×10^{-6}	This work
Pyrophyllite, diatomite (non-layered)	5.1×10^{-7}	8.34×10^{-6}	[25]
Pyrophyllite, diatomite (layered)	5.5×10^{-8}	2.78×10^{-6}	[25]
Fly ash, quartz	6.6×10^{-7}	0.63×10^{-5}	[27]
Alumina	1.0×10^{-7}	3.73×10^{-6}	[28]
Alumina	1.0×10^{-7}	1.39×10^{-6}	[29]
Kaolin, quartz	2.3×10^{-7}	0.37×10^{-6}	[30]
Fly ash	3.9×10^{-7}	4.33×10^{-5}	[31]
Kaolin, quartz	3.5×10^{-7}	1.94×10^{-6}	[32]

3.4. OW emulsion filtration

The permeate volume vs. normalized specific flux data for OW emulsion filtration are presented in Fig. 6. Even though the OW filtration experiments were performed under constant flux conditions, permeate fluxes decreased considerably due to membrane fouling by the OW emulsion. To consider permeate flux decline during membrane filtration, several researchers [48–50] have used normalized specific flux (N_f), which can be calculated as follows:

$$N_f = \frac{(J_t/P_t)}{(J_0/P_0)} \tag{13}$$

OW emulsion filtration experiments (Exps. 6, 7, and 8) were conducted at three different flow rates with a permeate volume of 0.4 L. The rejection rates for OW emulsions are presented in Table 1. In the case of Exp. 6 (OW emulsion concentration = 200 mg/L, flow rate = 8.33 × 10^{-7} m^3/s), the normalized specific flux decreased rapidly during filtration of the OW emulsion. The rejection rate for the OW emulsion was determined to be 90.4%. For Exp. 7 (OW emulsion concentration = 200 mg/L, flow rate = 1.67 × 10^{-6} m^3/s), the normalized specific flux dropped sharply to a rejection rate of 86.7%. In Exp. 8 (OW emulsion concentration = 200 mg/L, flow rate = 2.50 × 10^{-6} m^3/s), the normalized specific flux dropped quickly with a rejection rate of 91.8%. Our results indicated that the rejection rate of the OW emulsion was not affected by the applied flow rate under the given experimental conditions. Additional experiments (Exps. 9 and 10) were conducted with two different concentrations of OW emulsion and a filtration time of 90 min. In Exp. 9 (OW emulsion concentration = 50 mg/L, flow rate = 1.67 × 10^{-6} m^3/s), the normalized specific flux remained constant at 1.0 up to 0.5 L of permeate volume, decreased slowly to 1.5 L, and then dropped rapidly to 3 L. The rejection rate of Exp. 9 was determined to be 72.3% (Table 1). In Exp. 10 (OW emulsion concentration = 100 mg/L, flow rate = 1.67 × 10^{-6} m^3/s), the normalized specific flux decreased sharply up to 0.4 L of permeate volume and then fluctuated at low values (0.01–0.1) to 1.1 L. The rejection rate of Exp. 10 was 81.7% (Table 1), which was higher than that of Exp. 9.

Unlike the BSA solution, the rejection rates of OW emulsion were very high (72.3%–91.8%) under the given experimental conditions. This result was attributed to the size of the oil droplets. The droplet size distributions of OW emulsions with different oil concentrations are presented in Fig. 7. In general, the size of oil droplets depends on the amount of emulsifier and emulsification time [51]. In our experiments, the volume median diameter of the oil ranged between 160 and 530 nm for oil concentrations of 50, 100, and 200 mg/L, whereas the average oil droplet size ranged between 250 and 490 nm. The average diameters of oil droplets in the OW emulsions were higher than the pore diameter (220 nm) of the layered membranes. Therefore, oil droplets could not pass easily through the ceramic membranes during the filtration experiments. Similar findings have been reported by several researchers. Monash and Pugazhenthi [21] demonstrated that, under the given experimental conditions (OW emulsion concentration = 50–200 mg/L, oil droplet diameter = 50–4,000 nm), the rejection rates were very high (I support = 71%–96%, 3G support = 72%–96%, and 6G support = 83%–99%), showing a decreasing trend with an increase in applied pressure from 69 to 345 kPa. In addition, the rejection rate increased with an increase in OW emulsion concentration. For instance, the rejection rate of the 6G support (applied pressure = 69 kPa) increased from 92% to 99% with an increase in oil droplet concentration from 50 to 200 mg/L. They attributed this trend to the formation of larger oil droplets with an increase in oil droplet density. Suresh and Pugazhenthi [30] have fabricated ceramic membranes with fly ash and titanium dioxide to separate OW emulsions. Under the given experimental conditions (OW emulsion concentration = 200 mg/L, average oil droplet diameter = 6,928 nm), the ceramic membrane SP4 (average pore size = 2,280 nm) had rejection rates of 95.6%–99.2% for applied pressures ranging from 69 to 345 kPa. Cui et al. [52] have prepared NaA zeolite–alumina

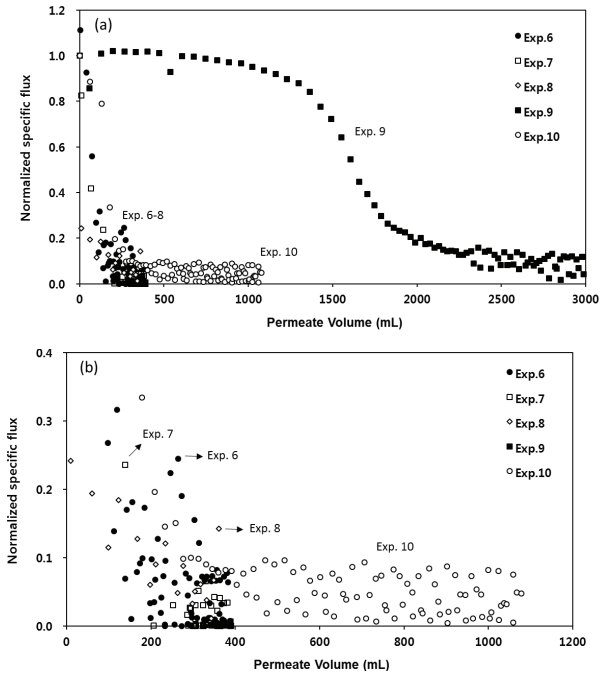

Fig. 6. Oil-in-water (OW) emulsion filtration: (a) permeate volume (0–3,000 mL) vs. normalized specific flux and (b) permeate volume (0–1,200 mL) vs. normalized specific flux.

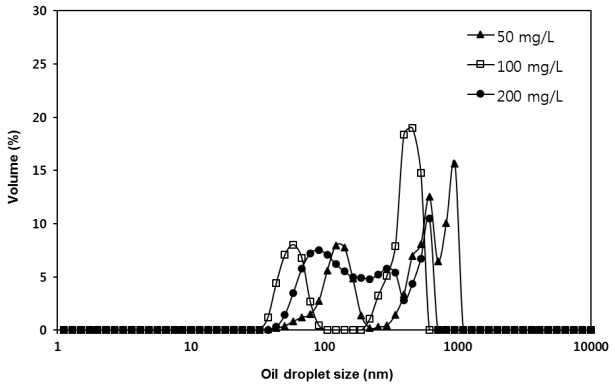

Fig. 7. Droplet size distribution of oil-in-water (OW) emulsion.

membranes with average pore sizes of 1,200 nm (NaA1), 400 nm (NaA2), and 200 nm (NaA3) to treat oil-contaminated water. They reported that both NaA1 and NaA2 membranes showed an oil rejection rate >97% under the given experimental conditions (OW emulsion concentration = 100 mg/L, average oil droplet diameter = 1,500 nm).

3.5. Combined fouling model analysis

The observed TMP data and the combined fouling model fits for Exp. 1 (BSA solution) are presented as an example in Fig. 8. The model parameters and error function values are provided in Table 4. Among the five combined fouling models (Eqs. (5)–(9)), the best-fit fouling model was chosen by comparing the values of three error functions (SAE, MPSED, and R^2). The cake-intermediate (CF-IB) model was most appropriate for describing the TMP data except for the cases of Exps. 3 and 5. The contributions of the cake filtration model and intermediate blocking model to the CF-IB model were calculated using the values of the fitted model parameters (K_cJ_0, K_i). The values of K_cJ_0/K_i for Exps. 1, 2, and 4 were calculated to be zero, indicating that the intermediate blocking model was a major component of the CF-IB model. Similar results were presented by Hlavacek and Bouchet [53], who performed membrane filtration experiments with BSA solution under constant flow rate conditions and reported that the pressure drop data were fitted best by the intermediate blocking model. The intermediate blocking model assumes that the particles do not necessarily block a membrane pore, and a particle in an aqueous solution can land on another particle previously deposited on the surface of the membrane [54,55]. For high flow rate conditions (Exp. 3) and high BSA concentrations (Exp. 5), the TMP data were most properly described by the cake-complete (CF-CB) model. The values of $K_cJ_0^2/K_b$ for Exp. 3 (8.7×10^3) and Exp. 5 (4.2×10^3) indicated that the cake filtration model was a major component of the CF-CB model. Angelis and de Cortalezzi [56] reported that membrane fouling was positively correlated with BSA concentration. They used ferroxane-derived ceramic membranes (average pore size = 76 nm) for BSA separation from aqueous solutions

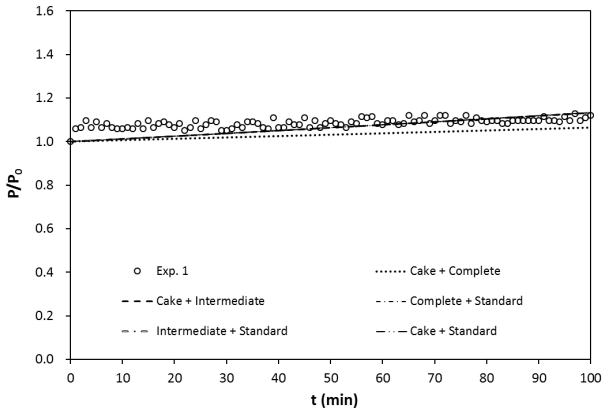

Fig. 8. Analysis of the combined blocking models for bovine serum albumin (BSA) solution filtration (an example of the model fits to Exp. 1). The model parameters and error function values are provided in Table 4.

(BSA concentration = 10, 100, 500, and 1,000 mg/L), showing that membrane fouling was minimal at a BSA concentration of 10 mg/L, but increased as the BSA concentration increased from 10 to 1,000 mg/L.

The observed normalized specific flux data and the combined fouling model fits for Exp. 6 (OW emulsion) are presented as an example in Fig. 9. The model parameters and error function values are provided in Table 5. The values of SAE, MPSED, and R^2 indicated that the CF-CB model was the most appropriate for describing the normalized specific flux data except for Exp. 9. The values of $K_cJ_0^2/K_b$ for Exp. 6 (5.4), Exp. 7 (17.5), Exp. 8 (28.0), and Exp. 10 (8.5) indicated that the cake filtration model was a major component of the CF-CB model. Vasanth et al. [41] have conducted OW emulsion filtration experiments using clay-based membranes at different pressures and flow rates, reporting that flux decline data were fitted best by the cake filtration model. Hu and Scott [57] have reported that the cake filtration model gave the best prediction for flux decline data obtained from the membrane filtration for the OW emulsion. The cake filtration model assumes that particles are not able to enter the membrane pores, but form a cake-like layer over the membrane surface [54]. In our experiments, oil droplets plugged and accumulated on the membrane pores to form a cake-like layer because the size of the oil droplets was larger than the pore size of the membrane. The value of $K_cJ_0^2/K_b$ increased with increases in flow rate and OW emulsion concentration, indicating that the contribution of the cake filtration model to membrane fouling increased with increases in flow rate and OW emulsion concentration. In the case of a low OW emulsion concentration (Exp. 9), the normalized specific flux data were most properly described by the CF-IB model. The value of K_cJ_0/K_i was 0.56, indicating that the contributions of the cake filtration model and intermediate blocking model to the CF-IB model were similar.

4. Conclusions

Ceramic microfiltration membranes were fabricated using pyrophyllite as a major support material. The FESEM images showed that the ceramic membranes were composed of a membrane support (thickness = 4 mm) and an alumina coating layer (thickness = 7.16 μm). Water permeation tests showed that the alumina-coated pyrophyllite membranes had a hydraulic permeability of 1.55×10^{-6} m^3/m^2 s kPa and an average pore radius of 1.1×10^{-7} m. The BSA filtration experiments demonstrated that the TMP values remained relatively constant throughout the BSA solution filtration. BSA particles had very low rejection rates (7.2%–16.1%) because the particle size of BSA was far smaller than the pore diameter of the membranes. The OW emulsion experiments showed that permeate fluxes decreased considerably due to membrane fouling by the OW emulsion. Oil droplets had very high rejection rates (72.3%–91.8%) because the size of oil droplets was larger than the membrane pore diameter. In the model analyses with five combined fouling models, most of the BSA filtration data were properly described by the cake-intermediate model, whereas most of the OW data were fitted best by the cake-complete model.

Table 4
Model parameters and error function values of combined blocking models for bovine serum albumin (BSA) solutions

Exp.	BSA concentration (mg/L)	Flow rate (m^3/s)	Combined model	J_0 (m/s)	K_b (s^{-1})	K_c (s/m^2)	K_i (m^{-1})	K_s (m^{-1})	SAE	MPSD	R^2
1	200	8.33×10^{-7}	CF-CB	1.8×10^{-5}	1.0×10^{-5}	3.1×10^{-15}	–	–	30.9	116.3	0.39
			CF-IB		–	0.0	1.2	–	**17.1**	**64.5**	**0.39**
			CB-SB		1.2×10^{-5}	–	–	4.6×10^{-1}	17.4	65.7	0.39
			IB-SB		–	–	1.2	0.0	17.1	64.5	0.39
			CF-SB		–	6.3×10^{-3}	–	1.2	17.3	65.4	0.39
2	200	1.67×10^{-6}	CF-CB	3.1×10^{-5}	2.4×10^{-5}	1.5×10^{-1}	–	–	4.3	24.6	0.61
			CF-IB		–	0.0	7.8×10^{-1}	–	**4.3**	**24.2**	**0.62**
			CB-SB		2.4×10^{-5}	–	–	1.0×10^{-3}	4.3	24.6	0.61
			IB-SB		–	–	4.5×10^{-3}	7.7×10^{-1}	4.3	24.4	0.62
			CF-SB		–	2.0×10^{-2}	–	7.7×10^{-1}	4.3	24.4	0.62
3	200	2.50×10^{-6}	CF-CB	5.2×10^{-5}	1.0×10^{-8}	3.2×10^{4}	–	–	**7.5**	**49.5**	**0.54**
			CF-IB		–	4.3×10^{-3}	1.6	–	7.7	51.0	0.53
			CB-SB		5.4×10^{-5}	–	–	4.5×10^{-1}	7.9	52.1	0.53
			IB-SB		–	–	1.6	0.0	7.7	51.0	0.53
			CF-SB		–	4.5×10^{-5}	–	1.5	7.8	51.8	0.53
4	500	1.67×10^{-6}	CF-CB	3.0×10^{-5}	2.8×10^{-5}	2.7×10^{-1}	–	–	27.5	100.2	0.76
			CF-IB		–	0.0	1.0	–	**26.4**	**96.1**	**0.77**
			CB-SB		1.0×10^{-11}	–	–	9.8×10^{-1}	26.9	98.1	0.77
			IB-SB		–	–	1.0	0.0	26.4	96.1	0.77
			CF-SB		–	3.5×10^{-5}	–	9.8×10^{-1}	26.9	98.1	0.77
5	1,000	1.67×10^{-6}	CF-CB	3.0×10^{-5}	1.0×10^{-8}	4.8×10^{4}	–	–	**31.4**	**111.3**	**0.83**
			CF-IB		–	0.0	1.3	–	33.1	117.3	0.82
			CB-SB		9.2×10^{-7}	–	–	1.2	33.9	120.4	0.82
			IB-SB		–	–	1.3	0.0	33.1	117.3	0.82
			CF-SB		–	0.0	–	1.2	33.9	120.4	0.82

Note: CF, cake filtration; CB, complete blocking; IB, intermediate blocking; SB, standard blocking. Bold values represent the error functions of the best-fit models.

Table 5
Model parameters and error function values of combined blocking models for oil-in-water (OW) emulsions

Exp.	OW concentration (mg/L)	Flow rate (m^3/s)	Combined model	J_0 (m/s)	K_b (s^{-1})	K_c (s/m^2)	K_i (m^{-1})	K_s (m^{-1})	SAE	MPSD	R^2
6	200	8.33×10^{-7}	CF-CB	1.4×10^{-5}	1.7×10^{-4}	4.6×10^{6}	–	–	**1.5**	**158.6**	**0.97**
			CF-IB		–	1.1	2.3×10^{1}	–	2.3	337.4	0.95
			CB-SB		1.8×10^{-4}	–	–	3.9×10^{-4}	2.7	425.0	0.94
			IB-SB		–	–	2.3×10^{1}	1.1×10^{-4}	2.3	337.4	0.95
			CF-SB		–	8.5×10^{-1}	–	1.7×10^{1}	2.5	369.4	0.95
7	200	1.67×10^{-6}	CF-CB	3.1×10^{-5}	1.7×10^{-4}	3.0×10^{6}	–	–	**0.5**	**328.2**	**0.99**
			CF-IB		–	8.9×10^{-4}	1.3×10^{2}	–	0.6	609.3	0.99
			CB-SB		1.7×10^{-4}	–	–	2.5 × 10	0.8	437.2	0.97
			IB-SB		–	–	2.2×10^{-3}	3.0 × 10	0.8	429.4	0.97
			CF-SB		–	8.9×10^{-4}	–	3.0 × 10	0.8	429.4	0.97
8	200	2.50×10^{-6}	CF-CB	4.6×10^{-5}	1.7×10^{-4}	2.2×10^{6}	–	–	**0.5**	**53.8**	**0.97**
			CF-IB		–	2.1×10^{6}	4.2×10^{-4}	–	0.5	55.8	0.97
			CB-SB		1.7×10^{-5}	–	–	3.1 × 10	0.8	79.2	0.92
			IB-SB		–	–	1.4×10^{-1}	7.1 × 10	0.8	97.4	0.96
			CF-SB		–	2.1×10^{6}	–	4.0×10^{-4}	0.5	55.8	0.97
9	50	1.67×10^{-6}	CF-CB	3.0×10^{-5}	1.7×10^{-14}	4.5×10^{5}	–	–	4.6	121.8	0.98
			CF-IB		–	9.6×10^{4}	5.1	–	**4.1**	**162.2**	**0.98**
			CB-SB		1.6×10^{-4}	–	–	1.1×10^{-4}	4.5	237.4	0.97
			IB-SB		–	–	2.5×10^{-6}	5.5	4.6	219.5	0.98
			CF-SB		–	4.0×10^{5}	–	3.7×10^{-1}	4.6	132.3	0.98
10	100	1.67×10^{-6}	CF-CB	3.1×10^{-5}	1.7×10^{-4}	1.5×10^{6}	–	–	**1.5**	**184.0**	**0.96**
			CF-IB		–	0.0	2.1×10^{-4}	–	8.1	1,388.1	0.89
			CB-SB		8.2×10^{-5}	–	–	3.0×10^{-4}	5.7	869.1	0.90
			IB-SB		–	–	1.3 × 10	3.5×10^{-4}	3.1	419.9	0.91
			CF-SB		–	6.0×10^{-5}	–	9.7×10^{-5}	8.1	1,388.2	0.89

Note: CF, cake filtration; CB, complete blocking; IB, intermediate blocking; SB, standard blocking. Bold values represent the error functions of the best-fit models.

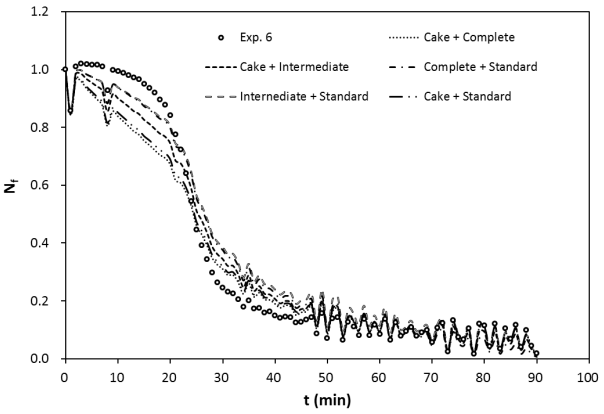

Fig. 9. Analysis of the combined blocking models for oil-in-water (OW) emulsion filtration (an example of the model fits to Exp. 6). The model parameters and error function values are provided in Table 5.

Acknowledgment

This work was supported by the National Research Foundation of Korea, funded by the Ministry of Education, Republic of Korea (grant number 2016-940823).

Symbols

A — Effective membrane area
C_i — Feed concentration
C_p — Permeate concentration
d — Membrane thickness
H_p — Hydraulic permeability
H_r — Hydraulic pore radius
J_0 — Initial permeate flux
J_t — Permeate flux at time t
n — Porosity
N_f — Normalized specific flux
P_0 — Initial transmembrane pressure
P_t — Transmembrane pressure at time t
Q — Flow rate
R — Rejection rate
t — Time
K_c — Characteristic constant of the cake filtration model
K_b — Characteristic constant of the complete pore blocking model
K_i — Characteristic constant of the intermediate pore blocking model
K_s — Characteristic constant of the standard blocking model
M_a — Mass of the water saturated membrane measured in water
M_d — Mass of the dried membrane
M_w — Mass of the membrane with pores filled with water
y_c — Calculated value from the model
y_e — Measured value from the experiment
$\overline{y_e}$ — Average of the measured value
μ — Water viscosity
ΔP — Transmembrane pressure

References

[1] N.L. Le, S.P. Nunes, Materials and membrane technologies for water and energy sustainability, Sustain. Mater. Technol., 7 (2016) 1–28.
[2] B. Hofs, J. Ogier, D. Vries, E.F. Beerendonk, E.R. Cornelissen, Comparison of ceramic and polymeric membrane permeability and fouling using surface water, Sep. Purif. Technol., 79 (2011) 365–374.
[3] J. Kim, B. Van der Bruggen, The use of nanoparticles in polymeric and ceramic membrane structures: review of manufacturing procedures and performance improvement for water treatment, Environ. Pollut., 158 (2010) 2335–2349.
[4] Y. Dong, J. Zhou, B. Lin, Y. Wang, S. Wang, L. Miao, Y. Lang, X. Liu, G. Meng, Reaction-sintered porous mineral-based mullite ceramic membrane supports made from recycled materials, J. Hazard. Mater., 172 (2009) 180–186.
[5] S. Jana, M.K. Purkait, K. Mohanty, Preparation and characterization of low-cost ceramic microfiltration membranes for the removal of chromate from aqueous solutions, Appl. Clay Sci., 47 (2010) 317–324.
[6] B.K. Nandi, A. Moparthi, R. Uppaluri, M.K. Purkait, Treatment of oily waste water using low-cost ceramic membrane: comparative assessment of pore blocking and artificial neural network models, Chem. Eng. Res. Des., 88 (2010) 881–892.
[7] P. Mittal, S. Jana, K. Mohanty, Synthesis of low-cost hydrophilic ceramic-polymeric composite membrane for treatment of oily wastewater, Desalination, 282 (2011) 54–62.
[8] P. Monash, G. Pugazhenthi, Development of ceramic supports derived from low-cost raw materials for membrane applications and its optimization based on sintering temperature, Int. J. Appl. Ceram. Technol., 8 (2011) 227–238.
[9] D. Vasanth, G. Pugazhenthi, R. Uppaluri, Fabrication and properties of low cost ceramic microfiltration membranes for separation of oil and bacteria from its solution, J. Membr. Sci., 379 (2011) 154–163.
[10] D. Vasanth, R. Uppaluri, G. Pugazhenthi, Influence of sintering temperature on the properties of porous ceramic support prepared by uniaxial dry compaction method using low-cost raw materials for membrane applications, Sep. Sci. Technol., 46 (2011) 1241–1249.
[11] D. Vasanth, G. Pugazhenthi, R. Uppaluri, Performance of low cost ceramic microfiltration membranes for the treatment of oil-in-water emulsions, Sep. Sci. Technol., 48 (2013) 849–858.
[12] S. Emani, R. Uppaluri, M.K. Purkait, Cross flow microfiltration of oil-water emulsions using kaolin based low cost ceramic membranes, Desalination, 341 (2014) 61–71.
[13] P.B. Belibi, M.M.G. Nguemtchouin, M. Rivallin, J.N. Nsami, J. Sieliechi, S. Cerneaux, M.B. Ngassoum, M. Cretin, Microfiltration ceramic membranes from local Cameroonian clay applicable to water treatment, Ceram. Int., 41 (2015) 2752–2759.
[14] J.K. Kang, C.G. Lee, J.A. Park, S.B. Kim, N.C. Choi, S.J. Park, Adhesion of bacteria to pyrophyllite clay in aqueous solution, Environ. Technol., 34 (2013) 703–710.
[15] A. Bentayeb, M. Amouric, J. Olives, A. Dekayir, A. Nadiri, XRD and HRTEM characterization of pyrophyllite from Morocco and its possible applications, Appl. Clay Sci., 22 (2003) 211–221.
[16] A. Talidi, N. Saffaj, K.E. Kacemi, S.A. Younssi, A. Albizane, A. Chakir, Processing and characterization of tubular ceramic support for microfiltration membrane prepared from pyrophyllite clay, Sci. Stud. Res.: Chem. Eng. Biotechnol. Food Ind., 12 (2011) 263–268.
[17] A. Agarwal, M. Pujari, R. Uppaluri, A. Verma, A novel method of reducing agent contacting pattern for metal ceramic composite membrane fabrication, Appl. Surf. Sci., 320 (2014) 52–59.
[18] C. Neelakandan, G. Pugazhenthi, A. Kumar, Preparation of NO_x modified PMMA-EGDM composite membrane for the recovery of chromium (VI), Eur. Polym. J., 39 (2003) 2383–2391.
[19] A. Majhi, P. Monash, G. Pugazhenthi, Fabrication and characterization of γ-Al_2O_3-clay composite ultrafiltration membrane for the separation of electrolytes from its aqueous solution, J. Membr. Sci., 340 (2009) 181–191.

[20] A.K. Basumatary, P.P. Adhikari, A.K. Ghoshal, G. Pugazhenthi, Fabrication and performance evaluation of fauhasite zeolite composite ultrafiltration membrane by separation of trivalent ions from aqueous solution, Environ. Prog. Sustain. Energy, 35 (2016) 1047–1054.
[21] P. Monash, G. Pugazhenthi, Effect of TiO_2 addition on the fabrication of ceramic membrane supports: a study on the separation of oil droplets and bovine serum albumin (BSA) from its solution, Desalination, 279 (2011) 104–114.
[22] D. Vasanth, K. Suresh, G. Pugazhenthi, Fabrication of circular shaped ceramic membrane using mixed clays by uniaxial compaction method for the treatment of oily wastewater, Int. J. Nano Biomater., 5 (2014) 75–88.
[23] R.V. Kumar, A.K. Ghoshal, G. Pugazhenthi, Elaboration of novel tubular ceramic membrane from inexpensive raw materials by extrusion method and its performance in microfiltration of synthetic oily wastewater treatment, J. Membr. Sci., 490 (2015) 92–102.
[24] J.H. Ha, J. Lee, I.H. Song, S.H. Lee, The effects of diatomite addition on the pore characteristics of a pyrophyllite support layer, Ceram. Int., 41 (2015) 9542–9548.
[25] J.H. Ha, S.Z.A. Bukhari, J. Lee, I.H. Song, S.H. Lee, The preparation and characterizations of pyrophyllite-diatomite composite support layers, J. Ceram. Soc. Jpn., 123 (2015) 1043–1050.
[26] J.H. Ha, S. Lee, S.Z.A. Bukhari, J.M. Lee, I.H. Song, The preparation and characterization of alumina-coated pyrophyllite-diatomite composite support layers, Ceram. Int., 43 (2017) 1536–1542.
[27] J.H. Kim, C.G. Lee, J.A. Park, J.K. Kang, N.C. Choi, S.B. Kim, Use of pyrophyllite clay for fluoride removal from aqueous solution, Desal. Wat. Treat., 51 (2013) 3408–3416.
[28] J.H. She, T. Ohji, S. Kanzaki, Oxidation bonding of porous silicon carbide ceramics with synergistic performance, J. Eur. Ceram. Soc., 24 (2003) 331–334.
[29] Y. Jeong, S. Lee, S. Hong, C. Park, Preparation, characterization and application of low-cost pyrophyllite-alumina composite ceramic membranes for treating low-strength domestic wastewater, J. Membr. Sci., 536 (2017) 108–115.
[30] K. Suresh, G. Pugazhenthi, Development of ceramic membranes from low-cost clays for the separation of oil-water emulsion, Desal. Wat. Treat., 57 (2016) 1927–1939.
[31] W.S. Ang, M. Elimelech, Protein (BSA) fouling of reverse osmosis membranes: implications for wastewater reclamation, J. Membr. Sci., 296 (2007) 83–92.
[32] J. Hermia, Constant pressure blocking filtration laws-application to power-law non-Newtonian fluids, Trans. Inst. Chem. Eng., 60 (1982) 183–187.
[33] C.C. Ho, A.L. Zydeney, A combined pore blocking and cake filtration model for protein fouling during microfiltration, J. Colloid Interface Sci., 232 (2000) 389–399.
[34] G. Bolton, D. LaCasse, R. Kuriyel, Combined models of membrane fouling: development and application to microfiltration and ultrafiltration of biological fluids, J. Membr. Sci., 277 (2006) 75–84.
[35] H. Razaei, F.Z. Ashtiani, A. Rouladitajar, Effects of operating parameters on fouling mechanism and membrane flux in cross-flow microfiltration of whey, Desalination, 274 (2011) 262–271.
[36] R. Golbandi, M.A. Abdi, A.A. Babaluo, A.B. Khoshfetrat, T. Mohammadlou, Fouling study of TiO_2-boehmite MF membrane in defatting of whey solution: feed concentration and pH effects, J. Membr. Sci., 448 (2013) 135–142.
[37] Y. Jafarzadeh, R. Yegani, M. Sedaghat, Preparation, characterization and fouling analysis of ZnO/polyethylene hybrid membranes for collagen separation, Chem. Eng. Res. Des., 94 (2015) 417–427.
[38] D. Wei, Y. Tao, Z. Zhang, X. Zhang, Effect of pre-ozonation on mitigation of ceramic UF membrane fouling caused by algal extracellular organic matters, Chem. Eng. J., 294 (2016) 157–166.
[39] Y. Yang, R. Chen, W. Xing, Integration of ceramic membrane microfiltration with powdered activated carbon for advanced treatment of oil-in-water emulsion, Sep. Purif. Technol., 76 (2011) 373–377.
[40] S.R.H. Abadi, M.R. Sebzari, M. Hemati, F. Rekabdar, T. Mohammadi, Ceramic membrane performance in microfiltration of oily wastewater, Desalination, 265 (2011) 222–228.
[41] D. Vasanth, G. Pugazhenthi, R. Uppaluri, Cross-flow microfiltration of oil-in-water emulsions using low cost ceramic membranes, Desalination, 320 (2013) 86–95.
[42] J. Fang, G. Qin, W. Wei, Z. Zhao, L. Jiang, Elaboration of new ceramic membrane from spherical fly ash for microfiltration of rigid particle suspension and oil-in-water emulsion, Desalination, 311 (2013) 113–126.
[43] B.K. Nandi, R. Uppaluri, M.K. Purkait, Treatment of oily waste water using low-cost ceramic membrane: flux decline mechanism and economic feasibility, Sep. Sci. Technol., 44 (2009) 2840–2869.
[44] M.Y. Wei, L.J. Leon, Y. Lee, D. Parks, L. Carroll, P. Famouri, Selective attachment of F-actin with controlled length for developing an intelligent nanodevice, J. Colloid Interface Sci., 356 (2011) 182–189.
[45] K. Hirayama, S. Akashi, M. Furuya, K. Fukuhara, Rapid confirmation and revision of the primary structure of bovine serum albumin by ESIMS and Frit-FAB LC/MS, Biochem. Biophys. Res. Commun., 173 (1990) 639–646.
[46] X. Ding, Y. Fan, N. Xu, A new route for the fabrication of TiO_2 ultrafiltration membranes with suspension derived from a wet chemical synthesis, J. Membr. Sci., 270 (2006) 179–186.
[47] D. Vasanth, G. Pugazhenthi, R. Uppaluri, Preparation, characterization, and performance evaluation of LTA zeolite–ceramic composite membrane by separation of BSA from aqueous solution, Sep. Sci. Technol., 52 (2017) 767–777.
[48] A.H. Nguyen, J.E. Tobiason, K.J. Howe, Fouling indices for low pressure hollow fiber membrane performance assessment, Water Res., 45 (2011) 2627–2637.
[49] D.T. Myat, M. Mergen, O. Zhao, M.B. Stewart, J.D. Orbell, S. Gray, Characterisation of organic matter in IX and PACl treated wastewater in relation to the fouling of a hydrophobic polypropylene membrane, Water Res., 46 (2012) 5151–5164.
[50] K. Kimura, K. Tanaka, Y. Watanabe, Microfiltration of different surface waters with/without coagulation: clear correlations between membrane fouling and hydrophilic biopolymers, Water Res., 49 (2014) 434–443.
[51] F. Dajnowiec, P. Banaszczyk, A. Kubiak, M. Biegaj, L. Zander, The study on oil droplet size distribution in O/W emulsions prepared by the use of the asymmetric membrane, Pol. J. Nat. Sci., 31 (2016) 665–680.
[52] J. Cui, X. Zhang, H. Liu, S. Liu, K.L. Yeung, Preparation and application of zeolite/ceramic microfiltration membranes for treatment of oil contaminated water, J. Membr. Sci., 325 (2008) 420–426.
[53] M. Hlavacek, F. Bouchet, Constant flowrate blocking laws and an example of their application to dead-end microfiltration of protein solutions, J. Membr. Sci., 82 (1993) 285–295.
[54] J.L. Soler-Cabezas, M. Torà-Grau, M.C. Vincent-Vela, J.A. Mendoza-Roca, F.J. Martínez-Francisco, Ultrafiltration of municipal wastewater: study on fouling models and fouling mechanisms, Desal. Wat. Treat., 56 (2015) 3427–3437.
[55] J.W. Son, E.H. Sim, N.C. Choi, S.B. Kim, C.Y. Park, Comparative analysis for fouling characteristics of river water, secondary effluent, and humic acid solution in ceramic membrane ultrafiltration, Sep. Sci. Technol., 52 (2017) 2199–2211.
[56] L.D. Angelis, M.M.F. de Cortalezzi, Ceramic membrane filtration of organic compounds: effect of concentration, pH, and mixtures interactions on fouling, Sep. Purif. Technol., 118 (2013) 762–775.
[57] B. Hu, K. Scott, Microfiltration of water in oil emulsions and evaluation of fouling mechanism, Chem. Eng. J., 136 (2008) 210–220.